# Enhancing Visible Light Photo-oxidation of Water with TiO2 Nanowire Arrays via Cotreatment with H-2 and NH3: Synergistic Effects between Ti3+ and N

**ARTICLE** *in* JOURNAL OF THE AMERICAN CHEMICAL SOCIETY · JANUARY 2012

Impact Factor: 12.11



**5 AUTHORS**, INCLUDING:

Sean P Berglund
Helmholtz-Zentrum Berlin
**21** PUBLICATIONS **544** CITATIONS

JACS
JOURNAL OF THE AMERICAN CHEMICAL SOCIETY

Communication

pubs.acs.org/JACS

# Enhancing Visible Light Photo-oxidation of Water with $TiO_2$ Nanowire Arrays via Cotreatment with $H_2$ and $NH_3$: Synergistic Effects between $Ti^{3+}$ and N

Son Hoang, Sean P. Berglund, Nathan T. Hahn, Allen J. Bard, and C. Buddie Mullins*

Departments of Chemical Engineering and Chemistry and Biochemistry, Center for Electrochemistry, Texas Materials Institute, Center for Nano- and Molecular Science, University of Texas at Austin, 1 University Station C0400, Austin, Texas 78712-0231, United States

Supporting Information

**ABSTRACT:** We report a synergistic effect involving hydrogenation and nitridation cotreatment of $TiO_2$ nanowire (NW) arrays that improves the water photo-oxidation performance under visible light illumination. The visible light (>420 nm) photocurrent of the cotreated $TiO_2$ is 0.16 mA/cm$^2$ and accounts for 41% of the total photocurrent under simulated AM 1.5 G illumination. Electron paramagnetic resonance (EPR) spectroscopy reveals that the concentration of $Ti^{3+}$ species in the bulk of the $TiO_2$ following hydrogenation and nitridation cotreatment is significantly higher than that of the sample treated solely with ammonia. It is believed that the interaction between the N-dopant and $Ti^{3+}$ is the key to the extension of the active spectrum and the superior visible light water photo-oxidation activity of the hydrogenation and nitridation cotreated $TiO_2$ NW arrays.

The search for cheap, efficient, and stable photocatalysts for solar hydrogen production from water splitting has been an increasingly active field since Honda and Fujishima's discovery of water photo-oxidation on a $TiO_2$ photoanode under ultraviolet (UV) light.[1] To date, $TiO_2$ is still one of the most studied photocatalyst materials due to its abundance, low cost, low toxicity, superior photostability, and high intrinsic catalytic activity under UV illumination.[2−5] However, the photoconversion efficiency of $TiO_2$ is limited to less than 2.2% under AM 1.5 global solar illumination due to its large band gap energy (3.0 eV for rutile and 3.2 eV for anatase).[6] The generally accepted benchmark for solar-to-hydrogen efficiency under AM 1.5 global illumination is 10% for practical implementation.[7] Therefore, extending the working spectrum of $TiO_2$-based materials to include more of the visible light region, which composes ∼45% of the total energy of the solar spectrum, has been of great interest.

Recent efforts have focused on modifying the valence band of $TiO_2$ by incorporating nonmetal ions such as C,[8] S,[9] and N.[4,10] The p states of the nonmetal foreign ions (N, S, or C) normally form impurity states above the valence band or hybridize with O 2p states (composing most of the valence band for $TiO_2$) thus upshifting the valence band edge of $TiO_2$.[3] Among nonmetal elements, N doping has been widely investigated and some success has been achieved in extending the working spectrum of $TiO_2$ toward the visible light range.[4] Modifying $TiO_2$ by hydrogen has also received attention recently.[11,12] Wang et al. demonstrated that annealing rutile $TiO_2$ nanowire (NW) arrays in a $H_2$ atmosphere creates oxygen vacancy sites thus forming donor states below the conduction band.[11] This improves light absorption and charge transport similar to n-type doping, thus enhancing water oxidation performance. Chen et al. reported a hydrogenation method to produce disorder in nanophase $TiO_2$, which significantly enhances visible light absorption.[12] Despite the interest in the effects of nitrogen doping and hydrogen modification, there are only a few studies on the synergistic effects of H and N codoping on the photocatalytic activity of $TiO_2$ materials.[13−17] To our knowledge, there is no report on the enhancement of visible light water photo-oxidation of $TiO_2$ due to the cotreatment with $H_2$ and $NH_3$ at high temperature. Diwald et al. prepared H, N-codoped $TiO_2$ material that is photoactive for Ag deposition under irradiation by photons of 2.4 eV by annealing rutile $TiO_2$ (110) in $NH_3$ at 870 K. The treatment introduced two species of N into the $TiO_2$ lattice: substitutional and interstitial N species.[17] The authors claimed that the codoping effect between the interstitial species and hydrogen is responsible for the enhancement in the visible light activity. The authors, however, did not consider the effects of $Ti^{3+}$ formation. In fact, under this nitridation condition, $Ti^{3+}$ formation is expected and can be more readily detected using bulk characterization techniques such as EPR rather than by conventional surface characterization techniques such as X-ray Photoemission Spectroscopy (XPS) due to the instability of the surface $Ti^{3+}$ in air or water.

In addition to enhancing optical absorption, it is equally important to optimize the photogenerated electron/hole separation characteristics. Vertically oriented nanocolumnar structures are considered to be very effective structures for photoelectrochemical (PEC) water splitting applications.[18,19] These structures permit significant light absorption depths while still enhancing the charge separation by providing high electrode/electrolyte interface areas and shortening the minority charge carrier transport distance to the electrolyte. We have recently reported the hydrothermal synthesis of vertically aligned ultrafine single crystalline rutile $TiO_2$ NW arrays with an average cross-sectional dimension of ∼5 nm.[10]

**Received:** December 5, 2011
**Published:** February 8, 2012





dx.doi.org/10.1021/ja211369s | J. Am. Chem. Soc. 2012, 134, 3659−3662

Upon nitridation in a $NH_3$ flow at 500 °C, the optical absorption and the PEC response spectrum extended from ~420 to ~550 nm. In the present study, we demonstrate synergistic effects of hydrogenation and nitridation that further extend the active spectrum of the $TiO_2$ NW arrays to ~570 nm. To our knowledge, we are the first to demonstrate the enhancement of visible light water photo-oxidation reactivity of $TiO_2$ material due to hydrogenation and nitridation cotreatment.

The $TiO_2$ photoelectrodes were prepared via two steps: (1) hydrothermal synthesis followed by (2) thermal treatments. The single crystalline rutile $TiO_2$ NW arrays with a thickness of 2.60 ± 0.27 $\mu$m were hydrothermally prepared on Fluorine-doped Tin Oxide (FTO) substrates. The NW arrays were further modified by annealing at 500 °C (i) in air for 1 h (denoted as $TiO_2$), (ii) in $NH_3$ for 2 h (N-$TiO_2$), (iii) in a mixture of $H_2$ and Ar (5% of $H_2$) for 1 h (H-$TiO_2$), and (iv) in a mixture of $H_2$ and Ar for 1 h followed by annealing in $NH_3$ for 2 h (H, N-$TiO_2$). Additional experimental details on the hydrothermal synthesis and thermal treatments can be found in the Supporting Information (SI).

The X-ray diffraction data (XRD) (SI, Figure S2a) confirm that all films are of rutile phase and no additional phase was detected upon thermal treatment. However, the thermal treatments have a profound effect on the visual appearance and morphology of the NW arrays. The white color of the pristine $TiO_2$ film did not change after hydrogen treatment; however, it turned green after nitridation and dark green after both treatments (SI, Figure S1). In addition the shape and size of the nanowires changed with each treatment as can be seen by the SEM images in Figure 1. Upon treatment, the cross

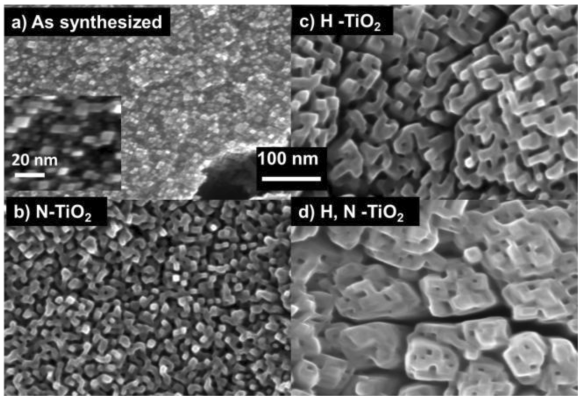


**Figure 1.** Scanning Electron Microscopy (SEM) images of (a) as-synthesized $TiO_2$ (inset shows higher magnification view), and films annealed at 500 °C in (b) $NH_3$, (c) $H_2$, and (d) $H_2$ and then $NH_3$.

section of the NW becomes larger due to the sintering of the small wires. Increases in the interplanar *d*-spacing for the (101) crystal plane due to cotreatment observed by Transmission Electron Microscopy (TEM) (SI, Figure S3) indicate lattice expansion as a result of N incorporation.

We employed X-ray Photoemission Spectroscopy (XPS) to investigate the chemical composition of the surface (Figure 2). The N 1s peak at 399.8 eV of the $TiO_2$ sample is assigned to molecular $N_2$ adsorbed on the surface.[4] The N 1s feature at 395.6 eV of the N-$TiO_2$ sample and the feature at 394.4 eV of the H, N-$TiO_2$ sample are assigned to substitutional $\beta$-N ($N^{3-}$) species which is considered responsible for enhancing the visible light activity of the N-doped materials.[4,20] It is

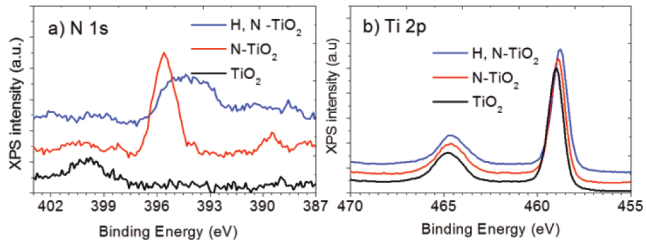


**Figure 2.** XPS spectra of the $TiO_2$, N-$TiO_2$, and H, N-$TiO_2$ NW arrays: (a) Core N 1s and (b) Core Ti 2p.

interesting that the N 1s feature of the H, N-$TiO_2$ sample is broader and shifts to a lower binding energy compared with that of the N-$TiO_2$. We will discuss these phenomena in more detail later. The substitutional N concentrations are calculated as 5.6 atomic % for N-$TiO_2$ and 3.5 atomic % for H, N-$TiO_2$, corresponding to $x$ values of 0.20 and 0.12 ($x$ in $TiO_{2-x}N_x$), respectively. The substitutional N concentration in our N-modified $TiO_2$ nanowires is considerably higher compared to other N-doped $TiO_2$ materials prepared via nitridation of $TiO_2$ at elevated temperature in a $NH_3$ flow.[21] The unique morphology and the ultrafine cross-section of the NW may enhance N diffusion into the $TiO_2$ lattice.

The Ti 2p3/2 XPS features are observed at 459.20, 458.76, and 458.71 eV for $TiO_2$, N-$TiO_2$, and H, N-$TiO_2$ respectively. These features are all assigned to $Ti^{4+}$, indicating no $Ti^{3+}$ species exist on the surface (the XPS technique characterizes the top 1−10 nm layer of the material). The presence of $Ti^{3+}$ was further investigated by low temperature electron paramagnetic resonance (EPR) (Figure 3). No EPR features appear

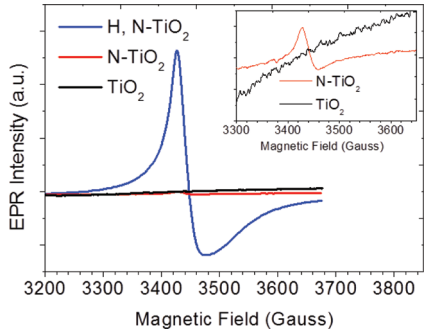


**Figure 3.** EPR spectra recorded at 86 K for $TiO_2$, N-$TiO_2$, and H, N-$TiO_2$ samples. The inset shows magnified view for the EPR spectra of the $TiO_2$ and N-$TiO_2$ samples.

for a *g*-value of ~2.02 corresponding to $O_2^-$ produced from the reduction of adsorbed $O_2$ (from air) by surface $Ti^{3+}$ further confirming the absence of surface $Ti^{3+}$.[22] Surface $Ti^{3+}$ is unstable under illumination in air or in electrolyte as it is easily oxidized by air or dissolved oxygen in water.[23] The strong EPR signal for a *g*-value of 1.992 for the H, N-$TiO_2$ sample indicates the presence of $Ti^{3+}$ in the bulk. We also observed a trace amount of $Ti^{3+}$ in the bulk of the N-$TiO_2$ sample. The intensity of the feature at a g-value of 1.981 for the N-$TiO_2$ sample is 2 orders of magnitude smaller than the feature at a *g*-value of 1.992 for the H, N-$TiO_2$ sample.

Linear sweep voltammetry (scan rate of 5 mV/s) results for the H, N-$TiO_2$ nanowires are shown in Figure 4a. The onset potential for the H, N-$TiO_2$ sample positively shifts to 0.6 V vs reversible hydrogen electrode ($V_{RHE}$) compared with 0.2 $V_{RHE}$


dx.doi.org/10.1021/ja211369s | J. Am. Chem. Soc. 2012, 134, 3659−3662

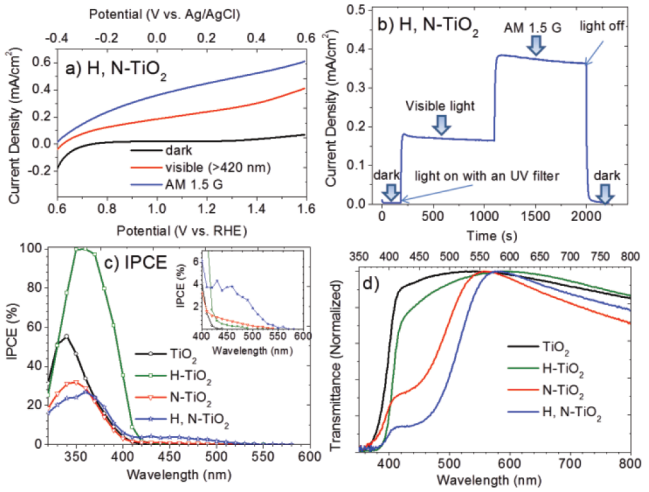


**Figure 4.** (a and b) Linear sweep voltametry (5 mV/s) and chronoamperometry at 1.23 $V_{RHE}$ of the H, N-$TiO_2$ sample, (c) IPCE spectra measured at 1.23 $V_{RHE}$, and (d) normalized transmittance spectra. All PEC measurements were performed using a three-electrode electrochemical cell with a Ag/AgCl reference electrode, a Pt wire counter electrode, and 1 M KOH electrolyte. A solar simulator (Oriel 96000) with an AM 1.5 G filter was used as the light source with a light intensity of 100 mW/$cm^2$ measured by a thermopile detector (Newport, 818P-020-12). A UV filter that blocks all wavelengths <420 nm was used for visible light experiments.

for the pristine $TiO_2$ sample even though the photocurrent transient onset potentials for the two sample are almost the same, ~ −0.15 $V_{RHE}$ (data not shown). The shift in the constant-illumination onset potential might be due to either a larger band bending requirement for separating electrons and holes because of the material's likely possession of poorer charge-transport properties than pure $TiO_2$ or slower surface kinetics as a result of hydrogenation and nitridation cotreatment.[10] The H, N-$TiO_2$ sample shows remarkable visible light water oxidation performance. The visible light (>420 nm) current reaches 0.159 mA/$cm^2$ at 1.23 V vs reversible hydrogen electrode ($V_{RHE}$) and contributes ~41% of the full AM 1.5 G photocurrent. The chronoamperometry (CAM) measurement at 1.23 $V_{RHE}$ (total time of ~30 min) in Figure 4b indicates the material's high stability. After the test, we observed the formation of bubbles on the film, suggesting the oxygen production from water oxidation. We believe that the formation of oxygen bubbles decreases the electrode/electrolyte contact area, resulting in a slight decrease of 4.6% in the AM 1.5 G photocurrent after 15 min of illumination. Figure S4 shows 3 runs of CAM measurements between which we used a pipet to flush out bubbles on the sample. The photocurrents were almost fully restored, thus supporting our hypothesis. In fact, after repeated testing for 5 months (the sample was stored in open air) the film still retains this performance. Figure 4c and d show the incident photon-to-current efficiency (IPCE) spectra and the normalized UV−vis transmittance spectra (the raw data are included in the SI, Figure S5). The absorption edge of the H, N-$TiO_2$ sample shifts ~20 nm to the longer wavelength region compared to the N-doped $TiO_2$ NW sample. The decrease in the transmittance for all samples at larger wavelengths than 570 nm is due to the light absorption of FTO substrates in this region which is confirmed by the UV−vis transmittance of FTO in Figure S5. The IPCE spectra fit well with the transmittance spectra, confirming that the active spectra of the H, N-$TiO_2$ sample extends to ~570 nm. The photocurrent obtained by integrating the calculated IPCE multiplied by the AM 1.5 G solar energy flux[24] over the range of 420−570 nm is 0.159 mA/$cm^2$, contributing to ~35% of the total integrated AM 1.5 G photocurrent (0.454 mA/$cm^2$). The small discrepancy between the full AM 1.5 G photocurrent obtained by the CAM measurement (0.388 mA/$cm^2$) and the integration method (0.454 mA/$cm^2$) might be due to the difference between the simulated sunlight (Xenon lamp + AM 1.5 G filter) and standard AM 1.5 G. The absence of a photoresponse in the IPCE of the untreated $TiO_2$ NW arrays indicates that the absorption tails from 420 to 500 nm in the transmittance spectra of the untreated $TiO_2$ sample are due to light scattering from the nanostructures. The H-$TiO_2$ sample shows significant improvement in the PEC performance in the UV region due to the enhancement in the electron conductivity.[11] Its IPCE spectrum, however, just shows a weak response from visible light (420 to ~500 nm), mainly due to the photoelectrochemically inactive transition from the valence band to hydrogenation-induced oxygen vacancy states.[11]

As mentioned in our previous study, incorporating N into the rutile $TiO_2$ NW arrays modifies the valence band structure, thus extending the working spectrum to ~550 nm. In the present study, we demonstrate that prehydrogenation significantly increases the bulk $Ti^{3+}$ concentration and the interaction between $Ti^{3+}$ and N-doping increases the visible light absorption and shifts the absorption edge further to the longer wavelength region (~ 570 nm) compared to individual doping with $Ti^{3+}$ or N. Employing EPR, Livraghi et al. detected paramagnetic bulk species of N ($N_b^{\cdot}$) at a $g$-value of 2.005, which formed localized states within the band gap of their N-doped $TiO_2$.[25] The authors proposed a reversible electron transfer between the $N_b^{\cdot}$ and $Ti^{3+}$ centers forming the diamagnectic bulk species of N ($N_b^-$) and $Ti^{4+}$. A similar phenomenon was also observed by Napoli et al. when they exposed a prereduced $TiO_2$ to a N plasma.[26] The N-induced states of $N_b^-$ species are higher in energy than that of corresponding $N_b$ species due to greater Coulombic repulsion. Di Valentin et al. prepared F, N-codoped $TiO_2$ samples and reported an increase in $Ti^{3+}$ concentration with an increasing F doping level. The authors also claimed that the formation of $N_b^-$ is more favorable with an increase in $Ti^{3+}$ and that is the key for the improvement in the visible light photocatalytic activity.[27] We did not detect any paramagnetic species other than $Ti^{3+}$ in our H, N-$TiO_2$ sample. We, however, can observe the interactions of $Ti^{3+}$ and substitutional N in the H, N-$TiO_2$ sample in the core N 1s XPS spectra (Figure 2a). The broadening and shift to the lower binding energy of the XPS N 1s feature compared with that of the N-$TiO_2$ sample indicates lower oxidation states of the substitutional N in the H, N-$TiO_2$ sample which might be due to electron transfer from $Ti^{3+}$. Due to the Columbic repulsion, the lower oxidation states of N in the H, N-$TiO_2$ sample have higher energy than that of the N-$TiO_2$ sample, thus enabling excitation with photons of longer wavelengths. The proposed interaction between $Ti^{3+}$ and N that modifies the electronic band structure of $TiO_2$ is illustrated in Figure 5.

In summary, we report a synergistic effect between hydrogen and nitridation cotreatment that significantly enhances the water photo-oxidation of rutile $TiO_2$ NW arrays under visible light. The photocurrent of the H, N-$TiO_2$ sample under visible light (>420 nm) illumination contributes ~41% of the


dx.doi.org/10.1021/ja211369s | J. Am. Chem. Soc. 2012, 134, 3659−3662

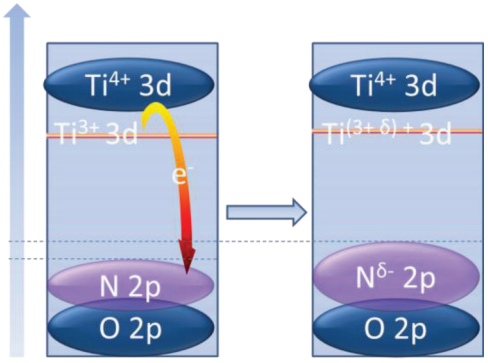


**Figure 5.** Proposed mechanism for the interaction between $Ti^{3+}$ and substitutional N.

simulated AM 1.5 G photocurrent. The IPCE and UV−vis transmittance spectroscopy reveal that the working spectrum of the H, N-$TiO_2$ sample extends to ∼570 nm compared with ∼550 nm for the N-$TiO_2$ and ∼420 nm for pristine $TiO_2$. The hydrogenation process increases the bulk $Ti^{3+}$ concentration in $TiO_2$. We speculate that the interactions between substitutional N and $Ti^{3+}$ are responsible for the enhancement in the water oxidation performance under visible light illumination.

## ■ ASSOCIATED CONTENT

### Supporting Information

Full experimental details, digital images, XPS, XRD, TEM, raw data of UV−vis transmittance, and the incident power density used in the IPCE measurements. This material is available free of charge via the Internet at http://pubs.acs.org.

## ■ AUTHOR INFORMATION

### Corresponding Author

mullins@che.utexas.edu

### Notes

The authors declare no competing financial interest.

## ■ ACKNOWLEDGMENTS

The authors gratefully acknowledge (i) the Division of Chemical Sciences, Geosciences, and Biosciences, Office of Basic Energy Sciences of the U.S. Department of Energy through Grant DE-FG02-09ER16119 and (ii) the Welch Foundation (C.B.M. for Grant F-1436 and A.J.B. for Grant F-0021). We would like to thank Minh Nguyen for help with EPR measurements and Vince Holmberg and Professor Brian Korgel for help with the UV−vis transmittance measurements.

## ■ REFERENCES

(1) Fujishima, A.; Honda, K. *Nature* **1972**, *238*, 37−38.
(2) Linsebigler, A. L.; Lu, G.; Yates, J. T. *Chem. Rev.* **1995**, *95*, 735−758.
(3) Chen, X.; Mao, S. S. *Chem. Rev.* **2007**, *107*, 2891−2959.
(4) Asahi, R.; Morikawa, T.; Ohwaki, T.; Aoki, K.; Taga, Y. *Science* **2001**, *293*, 269−271.
(5) Leary, R.; Westwood, A. *Carbon* **2011**, *49*, 741−772.
(6) Murphy, A. B.; Barnes, P. R. F.; Randeniya, L. K.; Plumb, I. C.; Grey, I. E.; Horne, M. D.; Glasscock, J. A. *Int. J. Hydrogen Energy* **2006**, *31*, 1999−2017.
(7) Bard, A. J.; Fox, M. A. *Acc. Chem. Res.* **1995**, *28*, 141−145.
(8) Park, J. H.; Kim, S.; Bard, A. J. *Nano Lett.* **2006**, *6*, 24−28.
(9) Umebayashi, T.; Yamaki, T.; Itoh, H.; Asai, K. *Appl. Phys. Lett.* **2002**, *81*, 454−456.
(10) Hoang, S.; Guo, S.; Hahn, N. T.; Bard, A. J.; Mullins, C. B. *Nano Lett.* **2012**, *12*, 26−32.
(11) Wang, G.; Wang, H.; Ling, Y.; Tang, Y.; Yang, X.; Fitzmorris, R. C.; Wang, C.; Zhang, J. Z.; Li, Y. *Nano Lett.* **2011**, *11*, 3026−3033.
(12) Chen, X.; Liu, L.; Yu, P. Y.; Mao, S. S. *Science* **2011**, *331*, 746−750.
(13) Mi, L.; Zhang, Y.; Wang, P. N. *Chem. Phys. Lett.* **2008**, *458*, 341−345.
(14) Russo, S. P.; Grey, I. E.; Wilson, N. C. *J. Phys. Chem. C* **2008**, *112*, 7653−7664.
(15) Pan, H.; Zhang, Y.-W.; Shenoy, V. B.; Gao, H. *J. Phys. Chem. C* **2011**, *115*, 12224−12231.
(16) Lan, M.; Peng, X.; Hong, S.; Pei-Nan, W.; Weidian, S. *Appl. Phys. Lett.* **2007**, *90*, 171909.
(17) Diwald, O.; Thompson, T. L.; Zubkov, T.; Walck, S. D.; Yates, J. T. *J. Phys. Chem. B* **2004**, *108*, 6004−6008.
(18) Hahn, N. T.; Ye, H.; Flaherty, D. W.; Bard, A. J.; Mullins, C. B. *ACS Nano* **2010**, *4*, 1977−1986.
(19) van de Krol, R.; Liang, Y. Q.; Schoonman, J. *J. Mater. Chem.* **2008**, *18*, 2311−2320.
(20) Takahashi, I.; Payne, D. J.; Palgrave, R. G.; Egdell, R. G. *Chem. Phys. Lett.* **2008**, *454*, 314−317.
(21) Wang, J.; Tafen, D. N.; Lewis, J. P.; Hong, Z.; Manivannan, A.; Zhi, M.; Li, M.; Wu, N. *J. Am. Chem. Soc.* **2009**, *131*, 12290−12297.
(22) Anpo, M.; Che, M.; Fubini, B.; Garrone, E.; Giamello, E.; Paganini, M. *Top. Catal.* **1999**, *8*, 189−198.
(23) Teleki, A.; Pratsinis, S. E. *Phys. Chem. Chem. Phys.* **2009**, *11*, 3742−3747.
(24) http://rredc.nrel.gov/solar/spectra/am1.5/.
(25) Livraghi, S.; Paganini, M. C.; Giamello, E.; Selloni, A.; Di Valentin, C.; Pacchioni, G. *J. Am. Chem. Soc.* **2006**, *128*, 15666−15671.
(26) Napoli, F.; Chiesa, M.; Livraghi, S.; Giamello, E.; Agnoli, S.; Granozzi, G.; Pacchioni, G.; Di Valentin, C. *Chem. Phys. Lett.* **2009**, *477*, 135−138.
(27) Di Valentin, C.; Finazzi, E.; Pacchioni, G.; Selloni, A.; Livraghi, S.; Czoska, A. M.; Paganini, M. C.; Giamello, E. *Chem. Mater.* **2008**, *20*, 3706−3714.